Power System Technology **Volume 46 · Number 4 · 2022**
ISSN: 1000-3673

Distribution Network Virtual Measurement Characteristics and Communication-assisted Protection Method Based on Sampling Value State Estimation

Cai Y., Cai Z., Li X., Zhao W., Ning N.

1. Hangzhou Polytechnic, Hangzhou, 311402, China
2. Beijing Ten Dimensions Technology Co., Ltd. Beijing, 100084, China
3. Hangzhou Vocational & Technical College, Hangzhou, 310018, China

ABSTRACT

The manufacturing process of complex chinaware combining 3D printing technology with traditional technology is studied. In this process, the ceramic artwork was divided into several components. The manufacturing process of each part of the green body was selected according to the shape, and then all the green bodies were fitted together through the assembly structure and interpenetrating network binder for biscuit firing (debinding), glazing and glaze firing. The composition ratio of ceramic slurry was adjusted to make its sintering shrinkage be the same as that of traditional ceramic slurry. The experiments gave the technological process and parameters, and its structures were analyzed by field emission scanning electron microscope. The influence factors of glue discharge process, microstructure and pore distribution of the printing body after glue discharge were studied, aiming to provide a basis for the popularization and application of the process.

1. INTRODUCTION

With the development of industrialization, the hand-made porcelain process is declining day by day, and the 3D printing technology has been developed vigorously [1]. More and more researchers have studied the 3D printing of ceramics [2], but less research on ceramic artwork. Xu and Zhou [3] made a complete surface of ceramic ring with the light curing technology. Jing Qiming used the combination of simulation design and traditional decoration technology to improve the decorative attributes of the work. Zeng et al. [4] studied the binder removal heat treatment process and sintering process of 3Dceramic printing. Prem et al. [5] studied the Mini-Extruder. However, combining3D printing technology with traditional porcelain making technology to produce complex shapes of ceramic artworks is rare, especially the glaze firing of 3D printing ceramics.

The ceramic body prepared by 3D printing after binder removal has low compressive strength, and it is not easy to moved and glaze. Since the density caused by high-temperature sintering exceeds 90%, it cannot adsorb the glaze. For the mass production of large-size porcelain, 3D printing has low production efficiency, high cost and low economy compared with traditional technology. Based on the fact that ceramic artworks with complex shapes can

be decomposed into one body and multiple attachments, this study aims to break the complex shapes of ceramic artworks, determine the manufacturing process of each attachments structure, make each attachment structure separately, glue the entire shape by binder using the Assembly structure, biscuit firing(de-binding), glazing, and glaze firing. For structural parts requiring 3D printing, the DLP printing technology is used to make the ceramic body. The sintering shrinkage is the same as that of the traditional clay according to adjusting the composition ratio of ceramic slurry. Combining traditional technology with modern technology, the company has developed a "manufacturing process of complex shaped ceramic artworks with multiple processes supported by 3D printing technology", making contributions to the promotion of porcelain manufacturing process and 3D printing technology.

2. OVERALL PROCESS

The technology mainly includes seven steps: (1) structural decomposition for complex modeling; (2) determine the manufacturing process according to the modeling of each part; (3) make ach decomposition structure separately;(4) combine Assembly structure and ceramic slurry into an integral shape; (5) biscuit firing (de-binding); (6) glazing; (7)Glaze firing. The vase in Fig.1 is taken as the test case.

Fig.1. A vase

3. STRUCTURAL DECOMPOSITION

According to the shape analysis, the basic shapes are classified according to the ceramic manufacturing process, and the whole shape is divided into multiple components. A large part that plays a supporting role in the whole is identified as the main body and the rest as attachments. General principles of decomposition are as follows:

Traditional process shall be selected as far as possible. 3D printing technology shall be adopted for the parts that are difficult to be manually made, with fine structure, small size or thin. Due to the slow printing speed of the current 3D printing technology, it is uneconomical to produce large-size structures.

The principle of convenient mold opening. The method of making mold through 3D printing, then the manufacturing of plaster mold and injection ceramic slurry is the most efficient and easy way. If this method can be used, it is recommended to use it as much as possible.

The assembly structure shall be set at the position where the main body has upward supporting attachments. To ensure the firmness of bonding, the shape damage during moving or glazing and the attachment displacement caused by glaze flow during glaze firing should be prevented. The assembly structure shall be set at the position where the main body has upward supporting attachments. To facilitate the later bonding operation, the number of decomposed components should not be too large. According to the above principles, the vase in Fig.1 can be divided into two parts: a revolving bottle and a flower, with the bottle as the main body and a flower as attachment.

4. BONDED ASSEMBLY STRUCTURE

There are two forms of bonding structure according to the size of the shape:

Wedge insertion form of convex column: for small shapes, only conical, pyramid and other convex column structures are designed on the attachments. When the main body was just dry and un-sticked, the convex column was inserted into the main body and a small amount of adhesive was applied to the joint, as shown in Fig. 2(a).

Convex concave fit form: For larger shapes, the convex concave structure of cone and pyramid shapes is adopted. The convex column is designed on the attachment. Before bonding, a pit with the same shape as the convex column at the corresponding position of the main body (the pit can be made directly during the casting process) is dug. During the bonding, the convex column is inserted into the pit and the adhesive is applied to the joint, as shown in Fig. 2 (b).

For the structure that does not allow relative rotation when the attachment part is assembled with the main body, the convex concave structure of pyramid shape shall be selected.

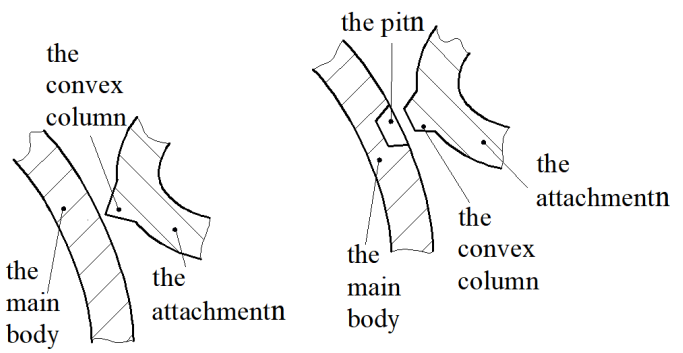

(a). Wedge insertion form of convex column (b) Convex concave fit form

Fig.2. Bonding structure

The vase bonding structure in Fig. 1 adopts the form of convex column insertion, and the flower handle is designed into a conical shape, as shown in Fig. 3.

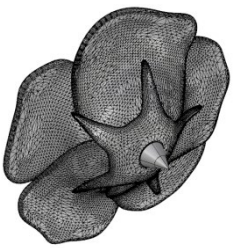

Fig.3. Bonding structure on the vase

5. SELECTION OF MANUFACTURING PROCESS BEFORE BONDING OF EACH DECOMPOSITION STRUCTURE

5.1. Ceramic 3D printing technology

Ceramic 3D printing technology is more and more mature with different processes [6]. Currently, there are 12 types of processes: direct writing forming DIW [7-8], ceramic clay extrusion disk forming CDM [9], stereo lithography (SLA) [10], digital light processing (DLP) [11], regional light transmission (LCD), selective laser sintering (SLS), selective laser melting (SLM), stereoscopic printing (3DP) [12], inkjet printing(IJP) [13], fused laminated forming (FDM) [14], layered solid forming (LOM), and two-photon polymerization (TPP) [15]. Among them, the printing parts manufactured by UV curing technology have high surface quality and moderate cost. When manufacturing ceramic artworks, light curing technology is selected. DLP and LCD technology are preferred because of their relatively low cost and fast printing speed. When making seed mold, photosensitive resin is used as printing material; when the attachments with small size and thin thickness are printed, ceramic slurry is used as the printing material through DLP or LCD technology.

5.2. Selection of different manufacturing processes according to the structural characteristics of each part

The structure and process flow applying for injection molding is 3D modeling, seed mold printing with resin, mold making with gypsum, and ceramic slurry injection manufacturing.

For the parts with complex shapes and wall thickness greater than 2mm, 3DP/SLA mode is for direct printing. For the parts with complex shapes and wall thickness less than 2mm, DLP/LCD mode is used for direct printing. The main structures with simple shapes and large size should be made by traditional methods or printed by CDM.

In this example, the flower is printed by 3D printing process, and the bottle body is made by traditional manual blank drawing or ceramic injection molding.

5.3. Fabrication of vase parts

5.3.1. The bottle body

The bottle body is made by grouting. The ceramic slurry is composed of 55% kaolin, 15% feldspar, 12% Longyan soil, 10% quartz and 8% Suzhou soil, and the firing shrinkage is 15%.

5.3.2. The flower

The maximum diameter of the flower 3D modeling is 500mm, and the average thickness of the petal is 1mm. Due to its small size and thin thickness, DLP technology is used for printing. The ceramic slurry in this experiment was mainly composed of ceramic powder and photosensitive resin premix [16]. The ceramic powder was kaolin powder with a particle size of D50=5.2um. The viscosity of the photosensitive resin premix was 20MPa·s, and the polyurethane prepolymer, active diluent HDDA, photo initiator and dispersant account for 25%, 60%, 1% and 14%, respectively.

On the basis that the rheological properties of the slurry meet the requirements of DLP, improving the solid loading of the light curing ceramic slurry is conducive to improving the printing accuracy [17]. It can also effectively avoid the defects such as green body cracking caused by excessive resin in the subsequent degreasing process, to obtain high-precision ceramic parts with complete surfaces and no defects. At low shear rate, the viscosity of slurry increases with the increase of solid content, and the relationship between solid loading and viscosity satisfies Krieger Dougherty model (See Eq.1.) [18-19].

$$\eta_r = (1 - \frac{\phi}{\phi_{max}})^{-m} \tag{1}$$

where: η_r is the relative viscosity value of ceramic slurry; Φ represents the solid content of ceramic slurry; $\Phi_{\max}$ is the highest solid content that can be achieved by the ceramic slurry theory, and m is the fitting parameter.

The maximum solid loading of slurry predicted by Krieger Dougherty model is 50.5% (volume fraction). The solid loading of the slurry used in this experiment was 50% (volume fraction) and the viscosity was 5600 MPa·s. Kaolin powder and photosensitive premixed liquid were mixed by mechanical mixing method, and then ball-milled with a planetary at a speed of 400 r/min for 2h. The ball material ratio was 3:2.

The AutoCera-M ceramic 3D printer is used. After printing, the printed pieces shall be ultrasonically cleaned and dried with alcohol.

6. BINDING

6.1. Producing binder

The binder was composed of 8 parts of ceramic slurry and 2 parts of interpenetrating binder, and the bonding strength was 26MPa.

The xylene [20] was heated in nitrogen atmosphere at 145℃; 1/2 amount of cross-linking agent [21] (allyl methacrylate) and acrylate monomer (the mixture of hydroxyethyl acrylate and iso-octyl acrylate with a mass ratio of 1:3) was added, and then 1/2 amount of initiator (ammonium persulfate aqueous solution) was dropped for 1.5 h.

Ceramic fiber (Al2O3) [22] was added to the remaining cross-linking agent to dip for 15min, and then added together into the reaction system as the above steps. After that, the initiator wad added to react for 6h, and the interpenetrating binder was obtained after filtering and drying.

The mass ratio of acrylate monomer, xylene, ceramic fiber, cross-linking agent and initiator was 50:25:10:1.5:0.3.

6.2. Bonding operation

After taking the bottle out of the plaster mold for about 2 hours, the conical convex column of the flower was inserted into the bottle to coat the joint with binder, and then the bottle and the flower were combined, as shown in Fig. 4.

Fig.4. Fit together

7. BISCUIT FIRING (DEBINDING) TEMPERATURE CURVE

The higher the sintering temperature [23], the greater the density of the green body [24]. Too high density of the green body will lead to the non-adhesion of glaze. As shown in Fig. 5, the annular ceramic part of 3D printing was fired at 1255℃ with a density of 93.5%, and the glaze did not adhere. The three exothermic characteristic peaks of the green body printed with ceramic slurry appeared at 276℃, 435℃ and 600℃ respectively, and the mass changed fast at 400℃. The first biscuit firing (de-binding) temperature curve was designed as follows: It was burned to 276℃ at a heating rate of 5℃ /min for 30min from room temperature, to 435℃ at a temperature-increasing rate of 1℃ /min for 30min, and then to 600℃ at a temperature-increasing rate of 5℃ /min for 30min. The second biscuit firing temperature curve is shown in Fig. 6. It was burned to 276℃ at a temperature-increasing rate of 3℃ /min for 60min from room temperature, to 435℃ at the heating rate of 1℃ /min and for 60min, to 600℃ at the heating rate of 3℃ /min for 60min, to 780℃ at the heating rate of 3℃ /min for 60min, and then reduced the temperature to 180℃ at the rate of 1℃ /min. The SEM photos of 3D printed green body after biscuit firing are shown in Fig. 7. From Fig. 7 (a), it can be seen that the grains after binder removal with the first biscuit temperature curve are large, distributed unevenly and have obvious layers. The second grain shown in Fig. 7 (b) is small and evenly distributed.

As shown in Fig. 8, the water adsorption of the vase under the second biscuit firing (de-binding) temperature curve was 10%-15%, and the strength of the green body was higher than that of the first one.

Fig.5. Glaze cannot adhere

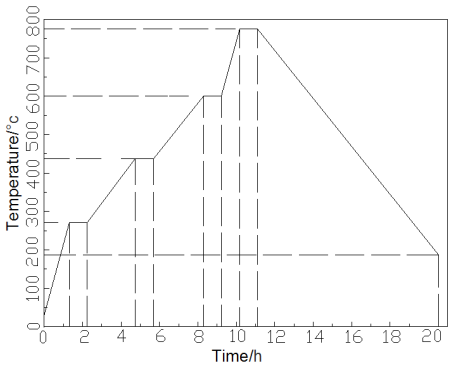

Fig.6. The second biscuit firing temperature curve

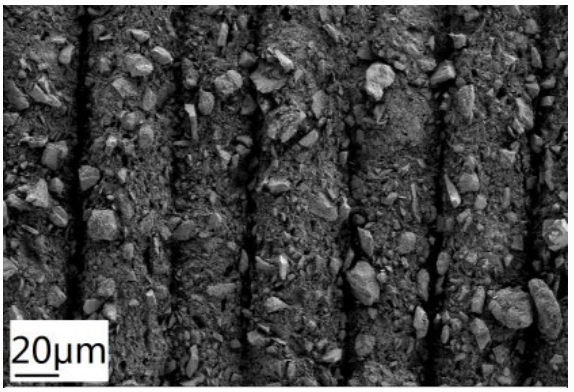

(a) SEM photos of the first process

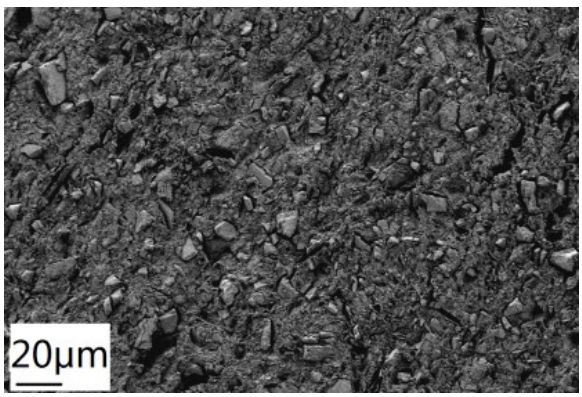

(b)

Fig.7. SEM photos after de-binding

Fig.8. The vase after bisque firing

8. GLAZING METHOD

Since the compressive strength of 3D printing part is lower after de-binding [25], the flow of glaze would cause the body cracking during the glaze firing. Since the flowers were placed horizontally, the vertical strength was low, as shown in Fig. 9. To reduce the support setting of the printing and the shape deformation caused by the glaze flow of the glaze firing, the shape of the 3D printing part should avoid having a large area of thin surface in the horizontal direction (the position during firing and printing). Glazing shall be done by spraying a small amount of glaze several times.

Fig.9. Horizontally placed flower

9. GLAZE FIRING TEMPERATURE CURVE

Considering the firing system of traditional clay and glaze, after many experiments, it is determined that the glaze firing temperature curve is shown in Fig. 10, and the maximum temperature is 1255℃. After firing, the thinnest part of the petal only has a thickness of 0.5mm, a bending strength of 118MPa, water absorption of 0.21%, and a glaze hardness of 8.

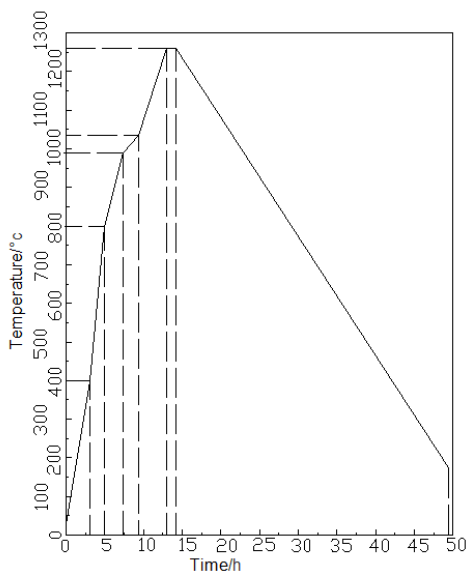

Fig.10. Glaze firing temperature curve

From the SEM photos of the glaze fired as shown in Fig. 11, it can be seen that the green body has fine structure, high density and only a small amount of blowhole.

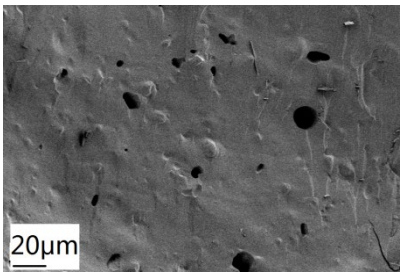

Fig.11. SEM photos of flower after glaze firing

10. CONCLUSION

Through the test, the following conclusions are drawn:

Before binder removal, the 3D printed Ceramic body has certain strength due to the resin, which can be bonded with the traditional clay body through a bonding structure. After binder removal, the strength is low, and the glaze can be carried out by the support of the main clay body.

The traditional ceramic biscuit firing process and the 3D printing ceramic binder removal process can be carried out at the same time to burn off moisture and organic matter, so that the 3D printing structure can adsorb the glaze.

The adhesive polymerized by interpenetrating network binder, inorganic particles and sodium silicate can form a strong anchoring structure between the ceramic body and attachment and the binder, which not only has strong adhesion, but also shortens the curing time.

Combined the traditional porcelain manufacturing process with modern technology, the multi-process composite manufacturing process integrated with 3D printing technology can produce ceramic artworks with complex shapes.

REFERENCES

[1] Meyers, S., De Leersnijder, L., Vleugels, J., & Kruth, J. P., Direct laser sintering of reaction bonded silicon carbide with low residual silicon content. Journal of the European Ceramic Society, 2018, 38(11): p. 33709-3717.

[2] Owen, D., Hickey, J., Cusson, A., Ayeni, O. I., Rhoades, J., Deng, Y., Zhang, Y., Wu, L.M., Park, H.Y., Hawaldar, N., Raikar, P.P., Jung, Y.G., Zhang, J., 3d printing of ceramic components using a customized 3d ceramic printer. Progress in Additive Manufacturing, 2018, 3(1-2): p. 3-9.

[3] Xu Y., Zhou Y.L., Exploration and practice on ceramic jewelry design supported by ceramic 3D printing technology. China Ceramics, 2021, 57(2): p. 77-81.

[4] Zeng Y., Zhang Z.J., Sun L.J., Yao H.H., Chen J.M., Atmosphere debinding heat treatment of 3D printed alumina ceramics. Journal of Inorganic Materials, 2022, 37(3): p. 33-337.

[5] Prem N., Sindersberger D., & Monkman G.J., Mini-Extruder for 3D Magnetoactive Polymer Printing. Advances in Materials Science and Engineering, 2019, 2019: p. 8715718.

[6] Srinivasan, D., Meignanamoorthy, M., Ravichandran, M., Mohanavel, V., Alagarsamy, S. V., Chanakyan, C., Rajkumar, S. 3D Printing Manufacturing Techniques, Materials, and Applications: An Overview. Advances in Materials Science and Engineering, 2021, 2021: p. 5756563.

[7] Coppola, B., Tardivat, C., Richaud, S., Tulliani, J. M., Montanaro, L., & Palmero, P., 3d printing of dense and porous alkali-activated refractory wastes via direct ink writing (DIW). Journal of the European Ceramic Society, 2021, 41(6): p. 3798-3808.

[8] Tan, J. J. Y., Lee, C. P., & Hashimoto, M., Preheating of gelatin improves its printability with transglutaminase in direct ink writing 3d printing. International Journal of Bioprinting, 2020, 6(4): p. 118-124.

[9] Jia Y.H., A Research Review on Innovative Design for Additive Manufacturing-Based Ceramics. Industrial& Engineering Design, 2021, 3(3): p. 13-19.

[10] Chen, Y., Furukawa, T., Ibi, T., Noda, Y., & Maruo, S., Multi-scale micro-stereolithography using optical fibers with a photocurable ceramic slurry. Optical Materials Express, 2021, 11(1): p. 105-114.

[11] Emir, F., & Ayyildiz, S., Accuracy evaluation of complete-arch models manufactured by three different 3d printing technologies: a three-dimensional analysis. Journal of Prosthodontic Research, 2021, 65(3): p. 365-370.

[12] Park, H. K., Shin, M., Kim, B., Park, J. W., & Lee, H., A visible light-curable yet visible wavelength-transparent resin for stereolithography 3d printing.NPG Asia Materials, 2018, 10(4): p. 82-89.

[13] Hasegawa, H., Inkjet printing and nanoscale electrocrystallization: complete fabrication of organic microcrystals-based devices under ambient conditions. Applied Materials Today, 2017, 9: p. 487-492.

[14] Medellin-castillo, H. I., & Zaragoza-Siqueiros, J., Design and manufacturing strategies for fused deposition modelling in additive manufacturing: a review. Chinese Journal of Mechanical Engineering, 2019, 32(3): p. 13-28.

[15] Ndinisa, S. S., Whitefield, D. J., & Sigalas, I., Fabrication of complex shaped alumina parts by gelcasting on 3D printed moulds. Ceramics International, 2020, 46(3): p. 3177-3182.

[16] Han Z.Q., Li L., Liu S.H., Qiu K., Wang S.X., & Liu F.T., Research on Rheological Properties of StereolithographyZrO, Ceramic Slurry. Bulletin of the Chinese Ceramic Society, 2021, 40(6): p. 1965-1971.

[17] Fuji, M., Inoue, Y., Takai, C., Nakashima, Y., & Ishihara, M., Simple analysis of adsorption amount of dispersant on ceramic slurry by capillary electrophoresis. Journal of the Society of Powder Technology Japan, 2017, 54(11): p. 725-731.

[18] Jongprateep, O., Wattana, N., Sato, N., Kien, P. T., & Inseemeesak, B., Effects of solid loading and silica addition on microstructure and compressive strength of hydroxyapatite specimens fabricated by freeze casting technique. Ceramics International, 2018, 44(1): p. S156-S160.

[19] Dehurtevent, M., Robberecht, L., Hornez, J. C., Thuault, A., Deveaux, E., & Béhin, P., Stereolithography: a new method for processing dental ceramics by additive computer-aided manufacturing. Dental Materials, 2017, 33(5): p. 477-485.

[20] Sun, L., Yuan, D., Liu, R., Wan, S., & Lu, X. Coadsorption of gaseous xylene, ethyl acetate and water onto porous biomass carbon foam pellets derived from liquefied Vallisnerianatans waste. Journal of Chemical Technology and Biotechnology, 2020, 95(5): p. 1348-1360.
[21] Boazak, E. M., Greene Jr, V. K., & Auguste, D. T., The effect of heterobifunctional crosslinkers on HEMA hydrogel modulus and toughness. PloS ONE, 2019, 14(5): p. 5890-5895.
[22] Abd Aziz, M. H., Othman, M. H. D., Hashim, N. A., Adam, M. R., & Mustafa, A., Fabrication and characterization of mullite ceramic hollow fiber membrane from natural occurring ball clay. Applied Clay Science, 2019, 177: p. 51-62.
[23] Wu, Z., Liu, W., Wu, H., Huang, R., He, R., Jiang, Q., Wu, S., Research into the mechanical properties, sintering mechanism and microstructure evolution of Al2O3-ZrO2 composites fabricated by a stereolithography-based 3D printing method. Materials Chemistry and Physics, 2018, 207: p. 1-10.
[24] Yıldız, B. K., Yılmaz, H., & Tür, Y. K., Influence of nickel addition on the microstructure and mechanical properties of Al2O3–5vol%ZrO2 ceramic composites prepared via precipitation method. International Journal of Minerals Metallurgy and Materials. 2019, 26(07): p. 908-914.
[25] Lombardo, S. J., & Retzloff, D. G., A process control algorithm for reaction-diffusion minimum time heating cycles for binder removal from green bodies. Journal of the American Ceramic Society, 2019, 102(3): p. 1030-1040.